Preprints.org

Article

Remarkably High 67.8 Dielectric Constant and 75 fF/μm2 Ni/ZrO2/TiN Capacitance Density Using Sub-Energy Bandgap Nanosecond Laser and Surface Plasma Effect

Wei Ting Fan , Pheiroijam Pooja , Albert Chin [*]

Article

Remarkably High 67.8 Dielectric Constant and 75 fF/µm² Ni/ZrO₂/TiN Capacitance Density Using Sub-Energy Bandgap Nanosecond Laser and Surface Plasma Effect

Wei Ting Fan, Pheiroijam Pooja and Albert Chin *

Department of Electronics Engineering, National Yang Ming Chiao Tung University, Hsinchu 300, Taiwan

* Correspondence: achin@nycu.edu.tw; Tel.: +886-3-5731841

Abstract: Rapid thermal annealing (RTA) has been widely used in the process of semiconductor devices. However, the rise time of RTA is limited by millisecond (ms) that is not suitable for advanced nanometre scale electron devices. Using sub-energy bandgap (E_G) 532 nm ultra-fast 15 nanosecond (ns) pulsed laser annealing, the record highest high dielectric constant (high-κ) of 67.8 and capacitance density of 75 fF/µm² at -0.2 V were obtained in Ni/ZrO₂/TiN capacitors According to the heat source and diffusion equations, the surface temperature of TiN can be as high as 870 °C at a laser energy density of 16.2 J/cm², which in turn anneals the ZrO₂ material. The record-breaking data are achieved by a new annealing method- the surface plasma effect generated on TiN metal. This is because the 2.3 eV (532 nm) pulsed laser energy is far below the 5.0~5.8 eV energy bandgap (E_G) of ZrO₂, which cannot be absorbed by the ZrO₂ dielectric. From X-ray diffraction analysis, the large κ value and capacitance density are attributed the crystallinity of cubic phase ZrO₂ that is improved with laser annealing and in turn improves the capacitance density. This technology is crucial for monolithic three-dimensional devices integration on the backend of advanced integrated circuit.

Keywords: high-κ; laser anneal; metal insulator metal; TiN; ZrO₂

1. Introduction

In the past decades, thermal annealing has progressed toward shorter cycles with higher temperatures. Crystallization by furnace requires high-temperature heat treatment, which causes long diffusion length and fails the small channel electron devices. To improve the impurity diffusion, Rapid Thermal Annealing (RTA) was used to replace the furnace annealing. Current spike RTA has a temperature ramp up at 400 °C/s to decrease the thermal diffusion effect.   One major limitation of spike RTA is that the irradiation energy must be larger than the energy bandgap (E_G) of the materials. However, the UV-visible light irradiation energy of RTA is lower than the wide E_G dielectrics in the backend of Integrated Circuits (ICs). Although indirect heating is available by Si substrate, the annealing effect on backend devices is insufficient. Besides, the maximum temperature for backend IC process is limited to 400 °C to prevent damage to frontend CMOS transistors.

In this study, we propose a new annealing method to improve the device quality for backend devices on isolation oxide. To further improve the impurity diffusion, a nanosecond (ns) pulsed laser is used. The proposed idea was verified by the large enhancement of 75 fF/µm² capacitance density and high dielectric constant (high-κ) of 67.8 by using 15 ns laser annealing, in the ZrO₂ metal-insulator-metal (MIM) device. These are the highest κ value and capacitance density reported in literature [1–3]. It is important to notice that the laser light energy significantly lower than energy bandgap of material, where the mechanism is due to the surface plasma effect [4] to create high-temperature on metal surface and heat up the ZrO₂ dielectric. The temperature profile under various laser annealing density is calculated using Matrix Laboratory (MATLAB). The peak temperature at TiN metal surface can be as high as 870°C, which can anneal above ZrO₂ dielectric efficiently. On the

other hand, the temperature is largely decreased below the 400°C within a TiN thickness of 30 nm, which meets the requirement with little effect on frontend CMOS transistors. This technology can improve the devices performance for Monolithic Three-Dimensional (M3D) integration on the backend of advanced Integrated Circuit (IC). Such M3D integration is crucible to improve the circuit speed and switching power consumption beyond the most advanced microprocessors [5–7].
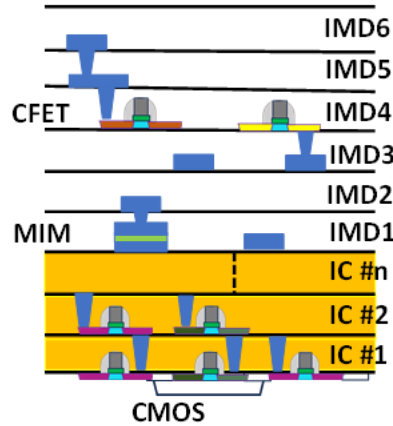
Figure 1. Monolithic Three-Dimensional (M3D) Integrated Circuit (IC).

2. Materials and Methods

A 50 nm TiN was first deposited and patterned as the bottom electrode for metal insulator metal (MIM) capacitor. Followed by NH_3^+ plasma treatment conditions under 2000 W (60 s and 120 s), 2400 W (60 s) and 2800 W (60 s) respectively to prevent capacitance-equivalent-thickness (CET) degradation by forming interfacial TiON during post-deposition annealing (PDA). Next, an 8 nm ZrO_2 layer was deposited via atomic layer deposition (ALD), and O_2-PDA at 400°C for 30 min to improve its dielectric quality. The ALD has a self-assembly mechanism with atomic layer-by-layer growth and precise thickness control. A HIPPO mid power Q-switched laser 532 nm with 5.4 J/cm², 16.2 J/cm² and 21.6 J/cm², was applied. Finally, a 50 nm Ni top electrode was deposited. The devices were characterized by capacitance density-voltage (C–V) and current density-voltage (J–V) measurements. Laser annealed (LA) samples was calculated using MATLAB to analyse temperature profile effectively. X-ray diffraction (XRD), Transmission electron microscope (TEM) and atomic force microscope (AFM) are used to understand the material quality and improvements.

3. Results

The heat diffusion equation governing the temperature evolution in both the TiN and ZrO_2 layers is given by:

$$\frac{\partial T}{\partial t} = \alpha \nabla^2 T + \frac{Q}{\rho c_p}, \tag{1}$$

$$\alpha = \frac{k}{\rho c_p}, \tag{2}$$

$$\nabla^2 T = \frac{\partial^2 T}{\partial r^2} + \frac{1}{r}\frac{\partial T}{\partial r} + \frac{\partial^2 T}{\partial z^2}, \tag{3}$$

Where α is the thermal diffusivity, $\nabla^2 T$ is the Laplacian of the temperature (describing the spatial derivatives of temperature in both radial and axial directions), k is thermal conductivity, ρ is material density, c_p is specific heat capacity, Q is the heat source term (which is zero for ZrO_2, but non-zero in TiN due to laser absorption). The heat is in a Gaussian profile in the radial direction because the laser beam typically has a Gaussian intensity profile. In the radial direction, the heat source term is expressed as:

$$Q = \frac{A_{TiN} T_{ZrO_2} E}{tA} \exp\left(-\frac{r^2}{2\sigma^2}\right) \tag{4}$$

$$T_{ZrO_2} = \frac{4n_1 n_2}{(n_1 + n_2)^2} \tag{5}$$

Where A_{TiN} is absorbance of TiN layer, T_{ZrO_2} is transmittance of ZrO_2, E is laser energy, A is spot size, t is laser irradiation time and σ is related to the focal radius, representing the width of the Gaussian beam profile, n_1 is the refractive index of ZrO_2 and n_2 is the refractive index of air. The ZrO_2 dielectric exhibited negligible absorption of laser energy, as its bandgap (5 to 5.8 eV) [8,9] significantly surpasses the photon energy of 2.33 eV. The increase in temperature can be attributed to the heat converted from the photon energy absorbed by TiN layer.

Figure 2 (a)-(c) present the simulation results of the temperature increase when laser irradiation with an energy density fluence of 5.4, 16.2 and 21.6 J/cm². TiN, a good plasmonic media is used as a metal layer to enhance the absorption of the irradiated pulse laser and diffuse the heat to ZrO_2 insulator layer above it [10,11]. The calculation displayed that the average temperature increases to 350 °C, 870 °C and 1450 °C at TiN surface and as heat diffuses, the temperature at ZrO_2 is 320 °C, 800 °C and 1300 °C, as the laser annealed energy density fluences are 5.4 J/cm², 16.2 J/cm² and 21.6 J/cm², respectively.


(a)

(b)

(c)
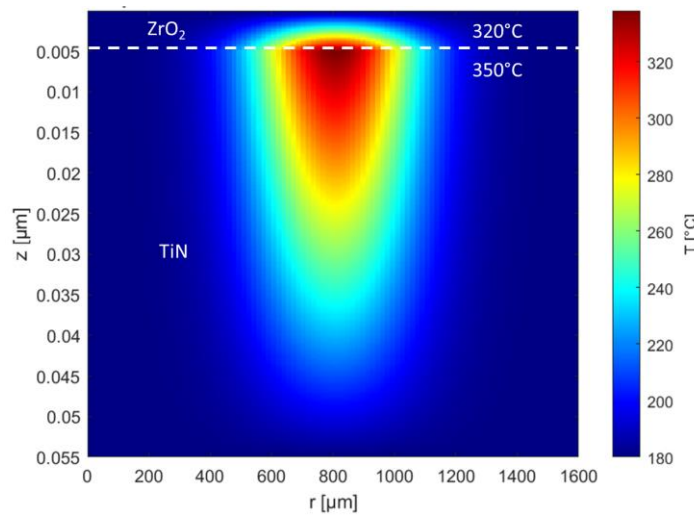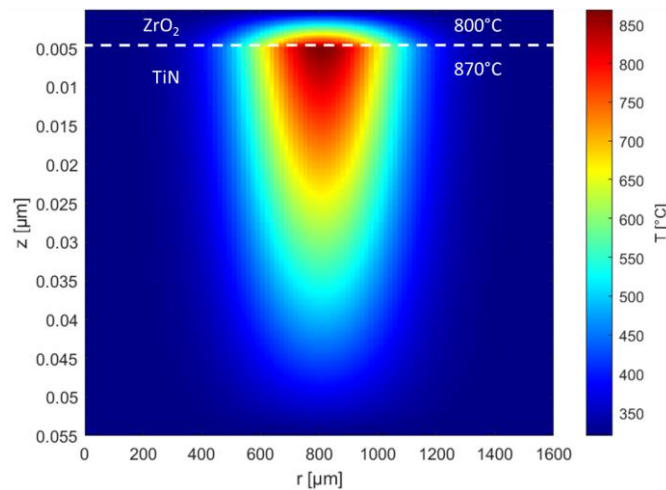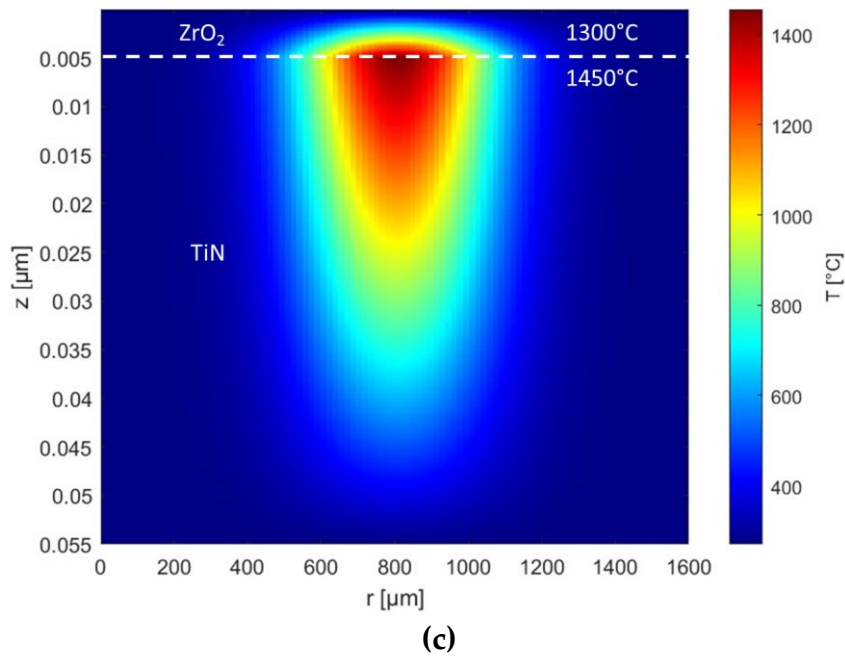
Figure 2. Temperature profile of TiN/ZrO$_2$ samples under 532 nm laser of (a) 5.4 J/cm^2 and (b) 16.2 J/cm^2 and (c) 21.6 J/cm^2.

Further, Lu et al. reported that ammonia (NH$_3$) plasma pre-treatment is crucial before the deposition of high-κ materials, as it significantly enhances interface properties [12]. Edwards et al. reported that NH$_3$ plasma treatment prior to SiN deposition significantly improves the degradation characteristics of AlGaN–GaN high-electron-mobility transistor (HEMTs) by reducing current collapse and eliminating gate lag after extended direct current bias [13]. This process strengthens bonds, making the structure more resistant to hot electron damage and passivating defects caused by it.
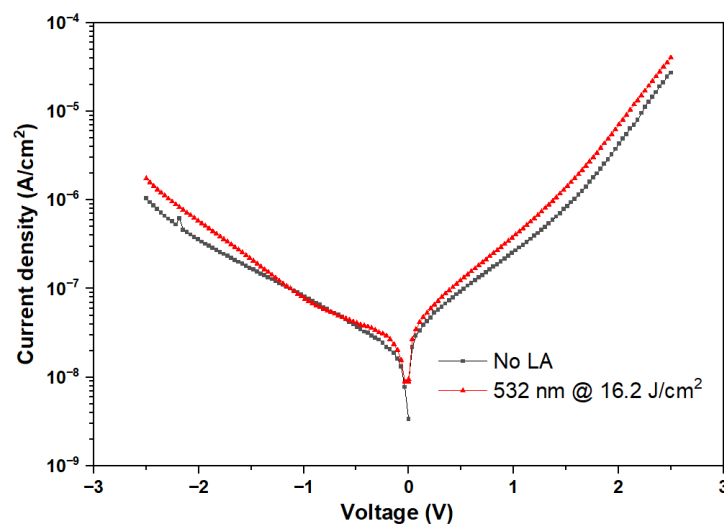
Figure 3 (a)-(d) shows the C–V characteristics of Ni/ZrO$_2$/TiN MIM capacitors before and after laser annealing under NH$_3^+$ plasma treatment conditions at 2000 W (60 s and 120 s), 2400 W (60 s) and 2800 W (60 s) respectively. The merits of using Ni electrode are the high work-function and reactive-ion-etching-friendly process [14]. For a 532 nm laser annealing with 2400 W 60s NH$_3^+$ plasma treatment in Figure 3 (c), the capacitance density increases monotonically with increasing laser-power that is 51.9 fF/um^2 for 5.4 J/cm^2 and 75 fF/um^2 for 16.2 J/cm^2 much better than the control devices before laser annealing, with a capacitance density of 41.7 fF/um^2 at -0.2 V. Therefore, the 2400 W 60s NH$_3^+$ surface treatment can make better formation and density of nitridation layer. Such nitridation layer can effectively prevent the ZrO$_2$ and TiN reaction at high temperature to form TiON. Under this condition, the plasma treatment significantly improves the TiN$_x$ surface for laser annealing. Other conditions, such as lower power (2000 W) or excessive power (2800 W), did not reach such high capacitance density due to either insufficient or excessive modification of the TiN$_x$ surface. Prolonged treatment times are less effective than the increased NH$_3^+$ plasma density. Thus, the 2400 W 60s NH$_3^+$ plasma condition represents an optimal balance on TiN surface nitridation, resulting in the best capacitance performance. Further when ZrO$_2$/TiN is laser annealed at 532 nm using 21.6 J/cm^2 energy density, it raises the temperature at TiN surface to 1450 °C and heat diffusion to ZrO$_2$ cause the temperature to raise to 1300 °C.
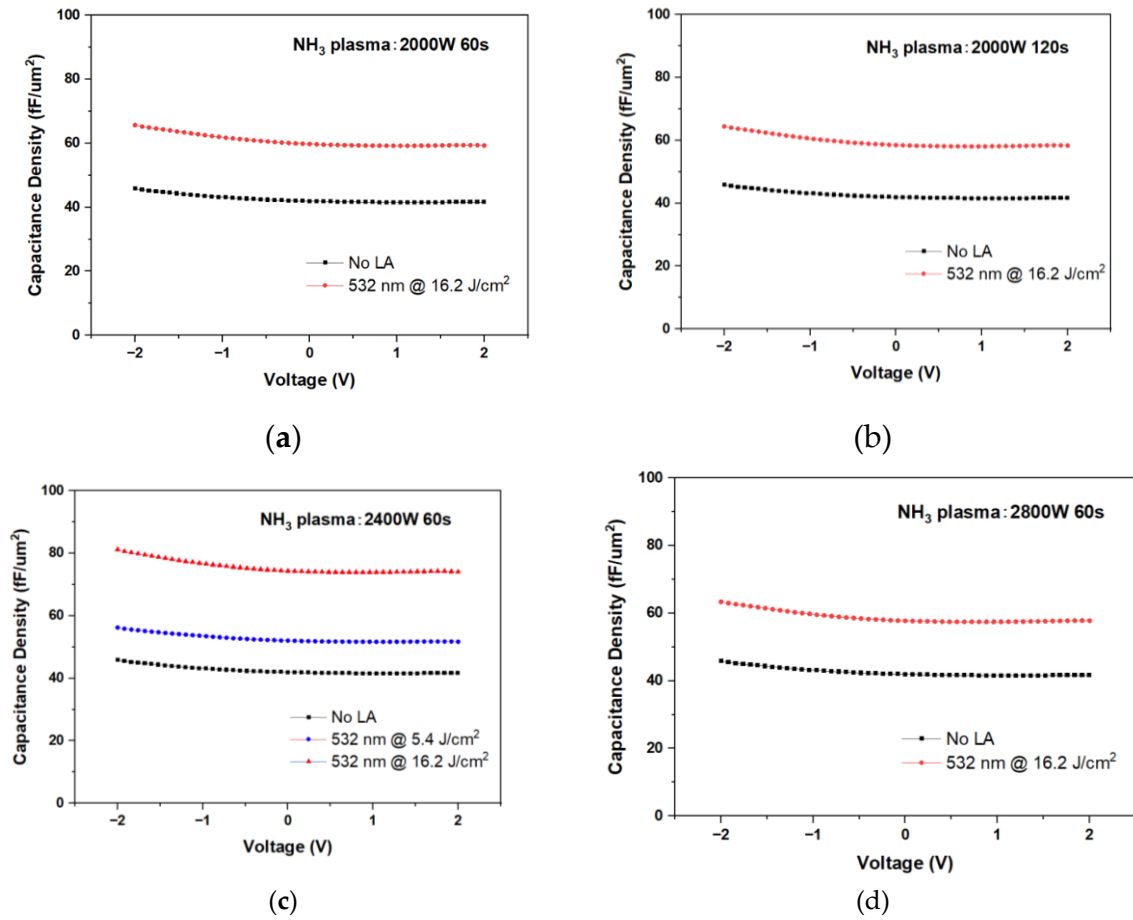
Figure 3. C–V of Ni/ZrO$_2$/TiN MIM capacitors under NH$_3^+$ plasma conditions (a) 2000 W 60s, (b) 2000 W 120s, (c) 2400 W 60s and (d) 2800 W 60s (LA: Laser annealed).

Figure 4 highlights the J–V plot of Ni/ZrO$_2$/TiN capacitor before and after laser annealing at 532 nm 16.2 J/cm^2. The leakage current increases slightly by 2.67×10^{-8} A/cm^2 at -0.2 V than the control devices before laser annealing, with leakage current of 2.17×10^{-8} A/cm^2 at -0.2 V.

Figure 4. J–V characteristics of the Ni/ZrO$_2$/TiN (LA: Laser annealed).

Figure 5(a) and 5(b) shows the C-V and (b) J-V analysis for Ni/ZrO$_2$/TiN MIM capacitors at higher 21.6 J/cm^2 laser annealing. No capacitance can be measured and the Ni/ZrO$_2$/TiN MIM device behaves like a small resistor. As shown in Figure 2(c), the temperature at TiN surface can raise to 1450 °C and heat diffusion to ZrO$_2$ cause the temperature to raise to 1300 °C. The laser energy is large enough and can cause thermal stress by local temperature rise exceeding the fracture strength of the film, the film will be wrinkled, cracked or even shed leading to failure of device [15]. Although these temperatures are still less than the melting temperature of ZrO$_2$ and TiN, such high temperature may cause ZrO$_2$ and TiN reaction, bond breaking, free Zr and Ti metals and shorting the capacitor.

(a)   (b)
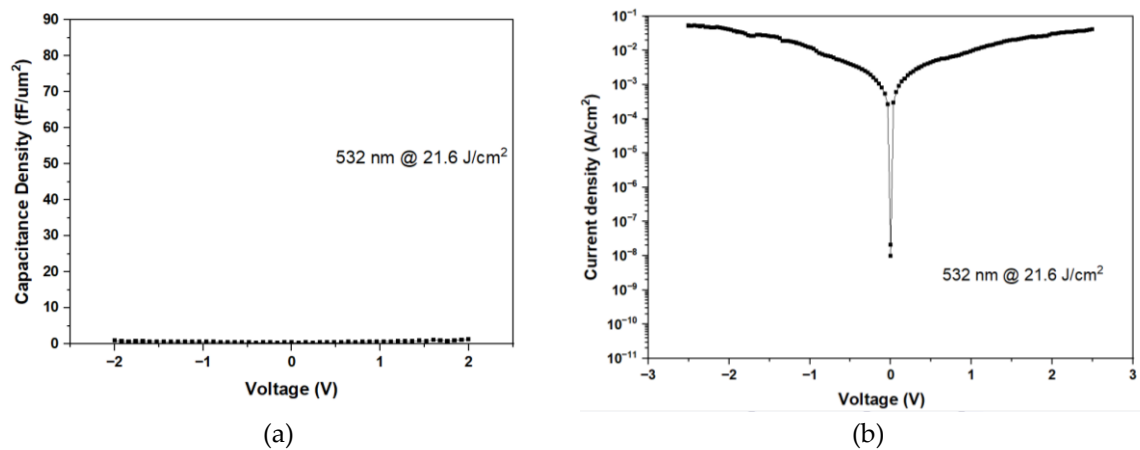
Figure 5. Ni/ZrO$_2$/TiN MIM capacitors laser annealed at 532 nm, 21.6 J/cm^2 (a) C-V and (b) J-V characteristics.

The slight increase in leakage current after laser annealing is attributed to larger grain size, as seen in XRD (Figure 6). The grain size of the ZrO$_2$ can be calculated by using Scherrer formula as

$$D = \frac{k\lambda}{\beta cos\theta} \qquad (6)$$

where D is the grain size, λ is the X-ray wavelength, k =0.9 is a dimensionless shape factor, β is the line broadening at half the maximum intensity (FWHM), and θ is the Bragg angle. The calculated grain sizes of ZrO$_2$, before and after laser annealing at 532 nm, 16.2 J/cm^2 is 6.85 nm and 8.21 nm respectively. This is similar to findings in TiO$_2$ MIM capacitors [16]. The annealing enhances ZrO$_2$ crystallinity, particularly in the high-κ cubic phase, evident from stronger XRD peaks. This improved crystallinity explains the higher capacitance density.
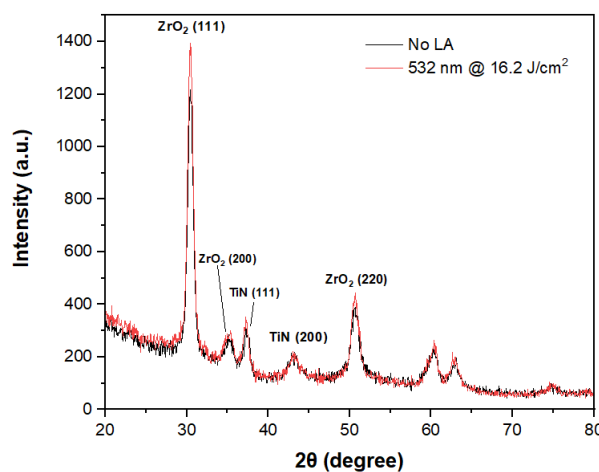

Figure 6. XRD spectra of the Ni/ZrO$_2$/TiN capacitors (LA: Laser annealed).

The TEM analysis is used to study the laser annealing condition. Figure 7 (a) and (b) further shows the cross-sectional TEM image of Al/ZrO$_2$/TiN structures before and after laser annealing. Clear better crystallization of ZrO$_2$ is observed after laser annealing, which is consistent with the XRD results. In the TEM image, the relatively rough top interface is Al rather than Ni. The samples analysed by TEM cannot contain magnetic substances such as iron/cobalt/nickel and other materials.

(a)   (b)
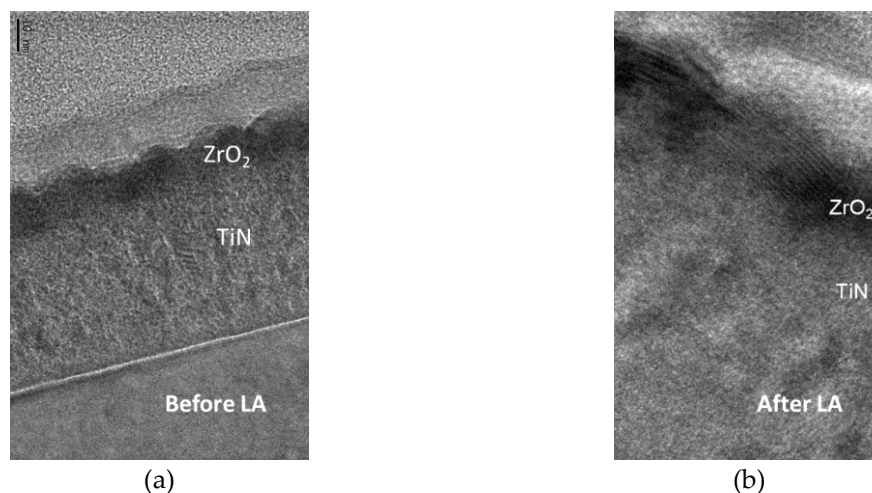
Figure 7. TEM cross sectional image of the Ni/ZrO$_2$/TiN capacitors (a) before and (b) after laser annealing.

The surface morphology of ZrO$_2$ before and after laser annealing samples is studied by AFM images, as shown in Figure 8 (a) and (b) using 5 μm × 5 μm scans. The root-mean-square roughness of ZrO$_2$ before laser annealing was found to be around 1.14 nm, whereas the roughness of the ZrO$_2$ after 532 nm laser annealing using 16.2 J/cm^2 was 1.25 nm. In the process of laser annealing, the raise in temperature enables the grain boundaries migration and causes more grains coalescence. More energy is available for the atoms to diffuse and lower surface energy grains get enlarge at high temperatures. The major growth in grain as observed from XRD analysis highlights the enhanced surface roughness for the laser annealed of ZrO$_2$ samples.

(a)   (b)
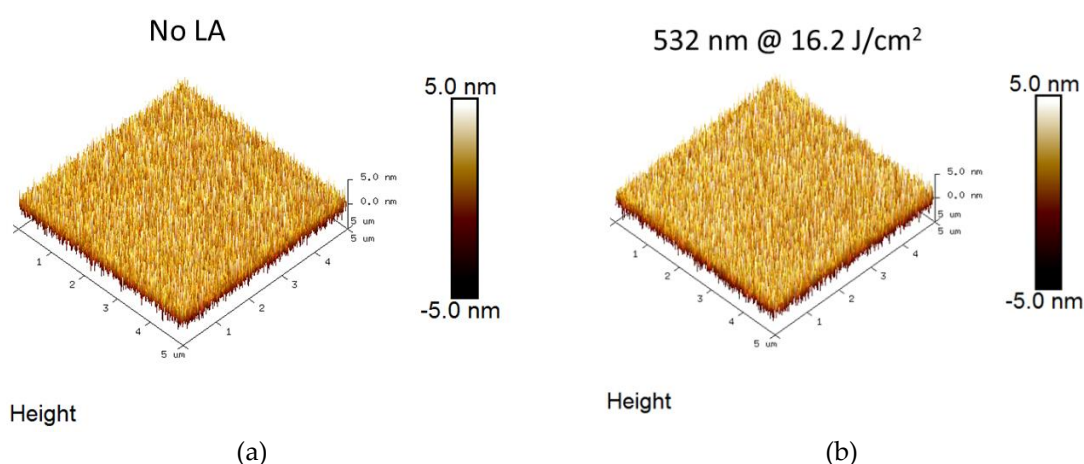
Figure 8. AFM images wide scans spectra of (a) No LA and (b) 532 nm LA, 16.2 J/cm^2 (LA: Laser annealed).

4. Conclusions

A high-performance Ni/ZrO$_2$/TiN device has been achieved, offering both increased capacitance density and low leakage current. MATLAB calculations confirmed that annealing temperature rises with increasing laser energy density, providing an alternative approach to achieve higher-κ

dielectrics for next-generation MIM capacitors without the need to constantly introduce new materials.

References

1. Kashir, A., Farahani, M. G., Kamba, S., Yadav, M., Hwang, H. $Hf_{1-x}Zr_xO_2/ZrO_2$ nanolaminate thin films as a high-k dielectric. *ACS Appl. Electron*. Mater. **2021**, 3 (12), 5632-5640.
2. Cheema, S.S., Shanker, N., Wang, LC., Hsu, C.H., et al. Ultrathin ferroic HfO_2–ZrO_2 superlattice gate stack for advanced transistors. *Nature*. **2022**, 604, pp. 65–71.
3. Tang, X., Li, Y., Miao, S., Chen, X., Xu, G., Lu, D., Long, S. Oxidizer engineering of ALD for efficient production of ZrO_2 capacitors in DRAM. *IEEE Electron Device Lett*. **2024**, 45, 2114-2117.
4. Hong, M., Dawkins, R.B., Bertoni, B., You, C, Magana Loaiza, O.S., Nonclassical near-field dynamics of surface plasmons. *Nat. Phys*. **2024**, 20, 830–835.
5. Yu, D.S., Chin, A., Laio, C.C., Lee, C.F., Cheng, C.F., Chen, W.J., Zhu, C., Li, M.F., Yoo, W.J., McAlister, S.P. Kwong, D.L. 3D GOI CMOSFETs with novel $IrO_2(Hf)$ dual gates and high-k dielectric on 1P6M-0.18μm-CMOS. In IEDM Technical Digest. IEEE International Electron Devices Meeting, San Francisco, CA, USA, 13-15 December 2004.
6. Shih, C.W., Chin, A., Lu, C.F., Yi, S.H. Extremely high mobility ultra-thin metal-oxide with ns^2np^2 configuration. IEEE International Electron Devices Meeting (IEDM), Washington, DC, USA, 07-09 December 2015.
7. Chin, A., Chen, Y.D. Technologies toward three-dimensional brain-mimicking IC architecture. Electron Devices Technology and Manufacturing Conference (EDTM), Singapore, 12-15 March 2019.
8. Sathyaseelan, B., Manikandan, E., Baskaran, I., Senthilnathan, K., Sivakumar, K., Moodley, M.K., Ladchumananandasivam, R., Maaza, M. Studies on structural and optical properties of ZrO_2 nanopowder for opto-electronic applications. *J. Alloys Compd*. **2017**, 694, 556-559.
9. Wilk G. D, Wallace R. M, Anthony J. M. High-k gate dielectrics: Current status and materials properties considerations. *J. Appl. Phys*. **2001**, 89(10), 5243- 5275.
10. Zhang, J., Chen, T.P., Li, X.D., Liu, Y.C., Liu, Y., Yang, H.Y. Investigation of localized surface plasmon resonance of TiN nanoparticles in TiN_xO_y thin films. *Opt. Mater. Express*. **2016**, 6(7), 2422-2433.
11. Kharitonov, A., Kharintsev, S. Tunable optical materials for multi-resonant plasmonics: from TiN to TiON. *Opt. Mater. Express*. **2020**, 10(2), 513-531.
12. Lu, H.L., Sun, L., Ding, S.J., Xu, M., Zhang, D.W., Wang, L.K. Characterization of atomic-layer-deposited Al_2O_3∕GaAs interface improved by NH_3 plasma pretreatment. *Appl. Phys. Lett*. **2006**, 89(15), 152910.
13. Edwards, A.P., Mittereder, J.A., Binari, S.C., Katzer, D.S., Storm, D.F., Roussos, J.A., Improved reliability of AlGaN-GaN HEMTs using an NH_3 plasma treatment prior to SiN passivation. *IEEE Electron Device Lett*. **2005**, 26(4), 225-227.
14. Chiang, K.C., Cheng, C.H., Jhou, K.Y., Pan, H.C., Hsiao, C.N., Chou, C.P., McAlister, S.P., Chin, A., Hwang, H.L. Use of a High-Work-Function Ni Electrode to Improve the Stress Reliability of Analog $SrTiO_3$ Metal–Insulator–Metal Capacitors. *IEEE Electron Device Lett*. **2007**, 28(8), 694-696.
15. Cao, Q., Su, J. Study on thermal effect and thermal stress effect of multilayer thin films induced by pulsed laser. In Pacific Rim Laser Damage 2019: Optical Materials for High-Power Lasers, 8 July 2019.
16. Chiang, K.C., Chin, A., Lai, C.H., Chen, W.J., Cheng, C.R., Hung, B.R., Liao, C.C. Very high K and high density TiTaO MIM capacitors for analog and RF applications. In Digest of Technical Papers. 2005 Symposium on VLSI Technology, Kyoto, Japan, 14-16 June 2005.